Influence of rake angle and nose radius on optical silicon nanomachining feed rate and surface quality: a modelling, prediction and optimisation study

Lukman N. Abdulkadir*,
Khaled Abou-El-Hossein
and Muhammad M. Liman

Precision Engineering Laboratory,
Nelson Mandela University,
6001, South Africa
Email: s215102134@mandela.ac.za
Email: Khaled.Abou-El-Hossein@mandela.ac.za
Email: s216651263@mandela.ac.za
*Corresponding author

Abstract: Silicon is widely used in infrared (IR) optics due to its high transmissive ability at wavelength (λ) ranging from 1.2 µm to 6.0 µm. However, optical components of high quality require surface roughness (Ra) below or equal to 8 nm. Ultra-high precision single-point diamond turning of optical silicon has filled this gap due to enhanced chip removal, well-defined grain structure and low coefficient of friction of diamond tool. This study aimed at reducing optical silicon Ra value by manipulating both cutting parameters and tool geometry. The recommended Ra value of less than 8 nm was achieved with standard runs 5, 6, 8, 9, and 10 respectively. Also, high surface roughness due to high feed rate was noted to be greatly reduced at high tool negative rake angle and nose radius. Additionally, with increase in tool nose radius at 0° rake angle, poor surface quality resulting from high feed rate reduced.

Keywords: optical silicon; surface roughness; subsurface damage response surface methodology; box Behnken; desirability function.

Reference to this paper should be made as follows: Abdulkadir, L.N., Abou-El-Hossein, K. and Liman, M.M. (2021) 'Influence of rake angle and nose radius on optical silicon nanomachining feed rate and surface quality: a modelling, prediction and optimisation study', *Int. J. Nanomanufacturing*, Vol. 17, No. 1, pp.47–75.

Biographical notes: Lukman N. Abdulkadir obtained his Bachelor and Master's degrees in the area of Mechanical Engineering and Production Engineering respectively from Abubakar Tafawa Balewa University Bauchi, Nigeria. He obtained his PhD in Mechatronics Engineering of the Nelson Mandela University in Port Elizabeth. He has published extensively in the field of high precision diamond turning of optical silicon. He has taught courses related to mechanical and mechatronics engineering and held several faculty posts. He is a Registered Engineer with the Council for the Regulation of Engineering in Nigeria (COREN) and corporate member of the Nigerian Society of Engineers (NSE).

Khaled Abou-El-Hossein obtained his Master and PhD from Ukraine in the areas of Machine Building Technology and Advanced Manufacturing. He is a Full Professor at Nelson Mandela University in South Africa. He has occupied several administrative positions which includes Head of Mechanical Engineering Department in Curtin University (Malaysia), Head of Mechatronics Engineering and Director School of Engineering in Nelson Mandela University. He has several publications in machining technologies and manufacturing of optical elements. He is registered with National Research Foundation of South Africa (NRF SA) and Engineering Council of South Africa (ECSA).

Muhammad M. Liman is a PhD student in the Mechatronics Department of Nelson Mandela University (NMU) in Port Elizabeth. He has published extensively in the field of high precision diamond turning of contact lens polymers. He obtained his Bachelor of Engineering from Bayero University Kano, Nigeria and graduated with *First Class Honours*. His Master's degree in the area of Mechatronics Engineering was from Nelson Mandela University where he graduated with Distinction (Cum laude). He is a Registered Engineer with the Council for the Regulation of Engineering in Nigeria (COREN) and corporate member of the Nigerian Society of Engineers (NSE).

1 Introduction

Optical components (infrared materials) are good material for imaging/illumination, medical, communication and measuring devices etc. (Faehnle et al., 2017; Abdulkadir et al., 2019). Optical components include: Aluminium oxynitride (AION), germanium, silicon and glass. Of these infrared materials, silicon has enjoyed extensive usage in infrared (IR) optics, solar cells and electronic devices which requires ultra-high precision and accuracy owing to its better transmissive ability across most infrared band (TOPSIL, 2013; Abou-El-Hossein, 2013; Yan et al., 2012). Surface roughness of optical materials is a significant manufacturing index and quality characteristic. Before a material is classed as good for optical purpose, its surface finish (R_a) is required to be below or equal to 8 nm (Mukaida and Yan, 2017; Ravindra and Patten, 2011; Yuan et al., 2017). Of the many methods employed to measure optical material surface roughness (R_a), stylus type method has gained wide usage due to its advantage in giving accurate numerical results (Hazir et al., 2018; Jumare et al., 2017, 2018). However, machining silicon is associated with slow processing speed, high tool wear and poor surface quality due to hardness.

Though other machining methods exist, turning has gained popularity over others being the most commonly used machining method in chip-based manufacturing industry. Therefore, numerous studies exist both in industrial and academic worlds on topics bothering on optimisation response factors such as tool wear, minimum roughness, vibration and tool temperature measurements etc. To deal with the highly needed form accuracy when machining silicon, ultra-high precision single point diamond turning of silicon (UHPDT) is now been used as an alternative to grinding and polishing. This is because diamond is known for its well-defined grain structure and low coefficient of

friction which enhances smooth sliding of chip over top rake angle keeping it away from the workpiece (Abdulkadir et al., 2018). Additionally, chip build-up, workpiece surface scratch and heat generation are either reduced or eliminated during cutting process thereby producing better surface finish than obtainable in lapping and polishing (Yergök, 2010; Luo et al., 2012). These advantages has made UHPDT a well sort for technique in optical fabrication than lapping and traditional polishing (Rhorer and Evans, 1995; Kumar et al., 2015).

In SPDT, adequate selection of feed rate, cutting speed, depth of cut (i.e., cutting parameters), rake angle, clearance angle and edge radius (i.e., tool geometry) is required. This would help to maintain ductile regime machining necessary for silicon surface integrity and high form accuracy (Jumare et al., 2017; Abdulkadir et al., 2018; Zhong, 2003). According to literature, (Abdulkadir et al., 2018) edge roundness increase leads to increase in tool rake angle negativity and uniform stress field with low concentration in the cutting region. The large negative effective rake angle created by the increase in edge roundness also further presses the materials in front of the cutting edge down in a compressive stress state (Yan et al., 2002). According to Yan et al. (2009), increasing edge radius leads to increase in thrust force and tool-chip temperature rise. The temperature rise shifts from rake to flank causing tool wear change from crater to flank. As further iterated by the same research group, material volume undergoing pressure increase as well as material elastic recovery are both increased while effective cutting gets reduced (Yan et al., 2009). The observed change in cutting condition linked to tool geometry, has led to several studies on the appropriate range which would not only ensure optically required surface roughness but also maintains ductility of optical silicon. According other researchers (Yan et al., 2001, 2002; Blake and Scattergood, 1990; Shibata et al., 1996), a –20 to –50° range negative rake angle is preferred for ductile mode machining while others (Fang and Zhang, 2003; Yan et al., 1999) documented that rake angle ranging from –60 to –80° are detrimental to optical silicon cutting.

In determining the most effective cutting condition for Si SPDT, these studies (Sata et al., 1985; Hocheng and Hsieh, 2004; Lee and Cheung, 2003; Sata, 2006; Kong et al., 2006) ranked feed rate, nose radius and depth of cut as superior over others, however, according to Jithin Babu and Babu (2014), surface roughness depends largely on feed rate than any other. Dogra et al. (2011) concluded that combining low feed rate, high cutting speed and large nose radius is the best for good surface finish. Although Zhang et al. (2014) said surface roughness is not affected by change in cutting speed if tool geometries and feed rates are appropriately chosen, however, according to Kandananond (2009), cutting speed is ranked as the next most important after feed rate . Interestingly, going by literatures consulted so far, combined effect of nose radius and rake angle as research parameter and optimisation on both roughness and feed rate level seems to be missing.

Owing to the above findings, tool-edge geometry and cutting parameters effects on surface integrity require to be understood. This would help to determine appropriate cutting conditions that can reduces roughness in order to achieve high form accuracy and integrity of optical surface. Therefore, for effective parametric and subsequent optimum level determination leading to reduced experimental trials and cost, this study considered feed rate, nose radius and rake angle as input factors. Also, for appropriate improvement

and prediction of surface quality, design of experiment (DOE)- an analytical based optimisation, was used due to the high success rate it has recorded in engineering field (Krimpenis et al., 2014; Asiltürk et al., 2016; Jacob and Banerjee, 2016).

2 Methods

Ultra-high precision turning was carried out on Precitech Nanoform ultragrind 250 machine as shown in Figures 1 and 2. Other details are shown in Table 1 based on the following literatures (Dogra et al., 2011; Ayomoh and Abou-El-Hossein, 2015; Fulemova and Janda, 2014; Tauhiduzzaman and Veldhuis, 2014).

Figure 1 Precitech nanoform 250 ultragrind (see online version for colours)

Figure 2 Experimental setup (see online version for colours)

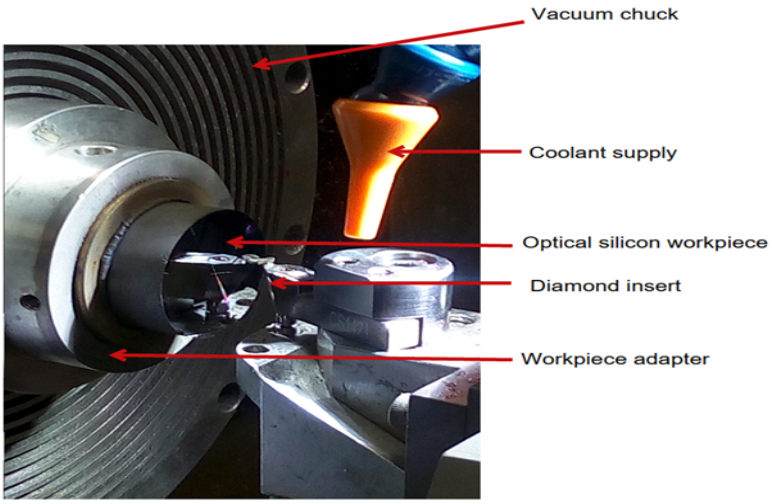

Table 1 Machining data

Material	*Information*
Workpiece	Optical grade (110) oriented single-crystal silicon (SCS) of 30 mm diameter and 14 mm thickness
Tool	Dodecahedral diamond cutting tool of (110) and (100) rake and flank faces with rake angles –40°, –25° and –0° nose radius 1.5, 1.0 and 0.5 mm; clearance angle–15°; side cutting edge angle 1—4°
Machine parameters	Cutting speed 750 rpm; feed rate 12, 7 and 2 mm/min; Depth of cut 17.5 µm
Coolant	Water

Using the data in Table 1, Box Behnken (BBD) technique was employed to generate the experimental design which gave the respective responses (Table 2) measured using a Form Talysurf PGI Optics 3D profilometer (Figure 3). BBD was used because it has no corner points, it is robust, good for non-sequential experimentation, offers efficient evaluation for first and second order models, requires minimal tests and almost rotatable (Dean and Voss, 1999; Ferreira et al., 2007). To study the effect of process parameters (γ, *R, f*), second-order regression mathematical model for surface roughness (Ra) based on RSM was developed (equations (1) and (2)).

$$W = \varphi(\gamma, R, f) \tag{1}$$

$$\hat{y}'' = y'' - \varepsilon = b_0 x_0 + b_1 x_1 + b_2 x_2 + b_3 x_3 + b_{11} x_1^2 + b_{22} x_2^2 + b_{33} x_3^2 + b_{12} x_1 x_2 + b_{13} x_1 x_3 + b_{23} x_2 x_3 \tag{2}$$

where W is the machinability aspect desired, φ response function, γ, R, f are rake angle, nose radius and feed rate , $\hat{y}''$ and y'' are the predicted and experimental value responses, x_0 = dummy variable and its equal to unity, $x_1 = rake\,angle$, x_2 = nose radius, $x_3 = feed\,rate$, ε = experimental error, while b_0, b_1, b_2, b_3 are the model parameters.

Figure 3 Stylus probe of form Talysurf PGI optics 3D profilometer (see online version for colours)

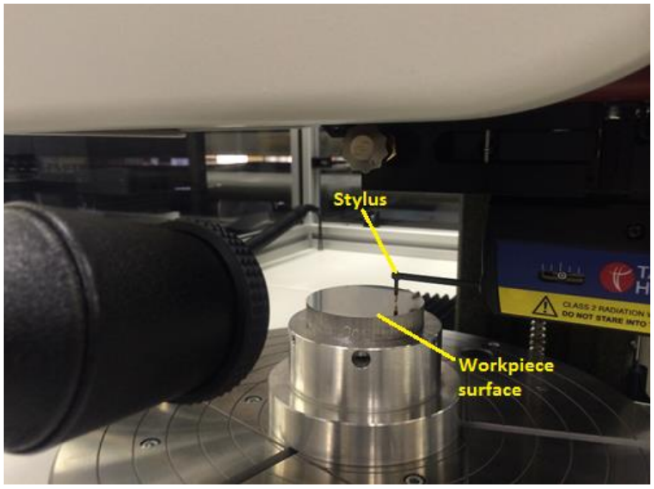

Table 2 BBD and responses

Expt. Run	*Factor 1*	*Factor 2*	*Factor 3*	*Response*
	Rake angle (Degree)	*Nose radius (mm)*	*Feed rate (mm/min)*	R_a *(nm)*
1	–25	1.5	12	*32*
2	–25	1	7	*26.5*
3	–25	1	7	*26.5*
4	0	1.5	7	*11.4*
5	0	1	12	*135*
6	–25	1	7	*26.5*
7	–40	1.5	7	*8*
8	–25	1	7	*26.5*
9	0	0.5	7	*68*
10	–25	0.5	2	*2.5*
11	–40	1	12	*7*
12	–40	0.5	7	*60*
13	–25	1	7	*26.5*
14	–40	1	2	*2.3*
15	0	1	2	*1.8*
16	–25	0.5	12	*130*
17	–25	1.5	2	*3*

The lowest and highest roughness values of optical silicon surfaces as obtained from Talysurf PGI profilometer measurements and workpiece surfaces are presented in Figures 4–7.

Figure 4 Surface profile chart for R_a 1.8 nm (see online version for colours)

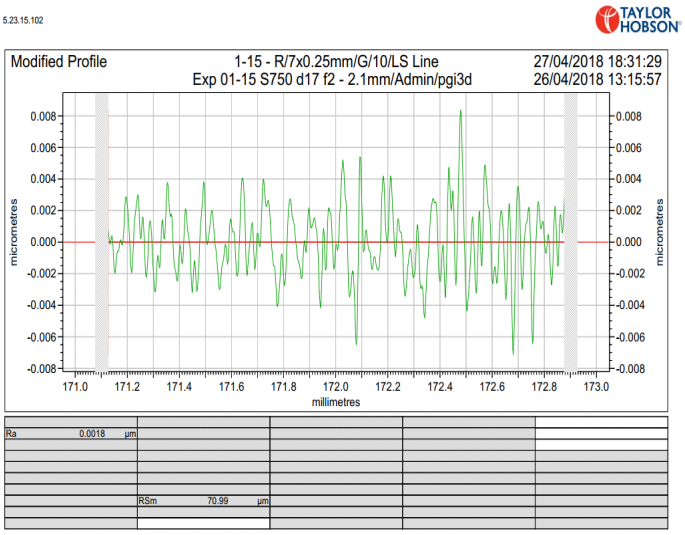

Figure 5 Mirror surface at R_a 1.8 nm (see online version for colours)

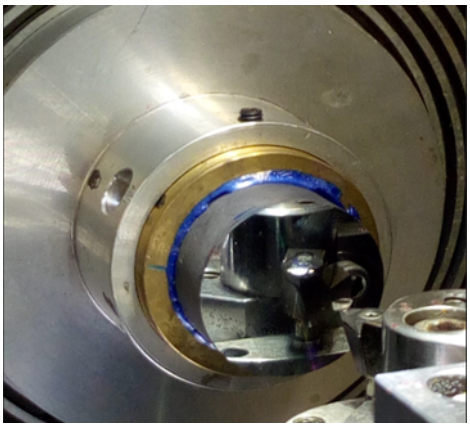

Figure 6 Surface profile chart for R_a 135 nm (see online version for colours)

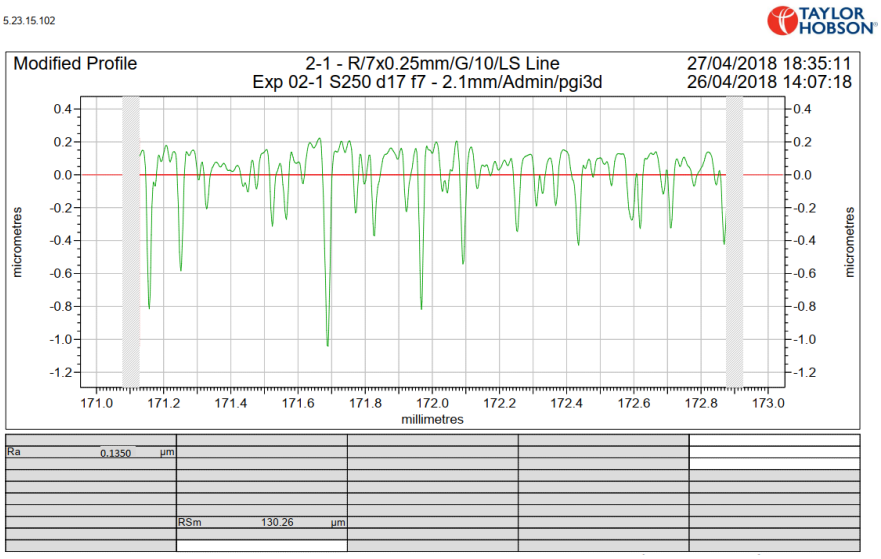

Figure 7 Workpiece **s**urface at R_a 135 nm (see online version for colours)

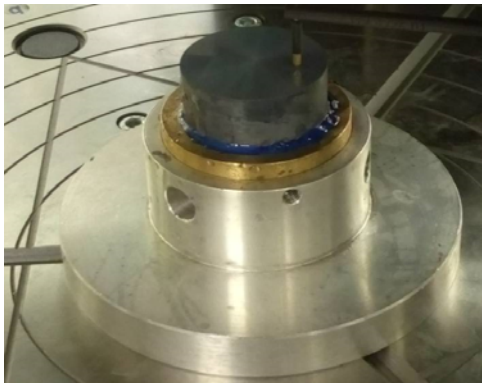

3 Results and discussion

3.1 Model prediction and statistical analysis

Using Box-Cox plotting technique, the inverse square root (equation (3)) power transformation for modelling surface roughness was suggested. The use of Box-Cox (Figure 8) to select transformation model became necessary because of the maximum to minimum response ratio which was greater than 10 (Stat-Ease Inc USA, 2008). The final model for surface roughness prediction is given in equations 4. Inverse square root model suggested means that the square root of the variance of the errors is linearly relatable to the level of the original series (http.//fmwww.bc.edu/repec/bocode/t/transint.html). The model adequacy and the significance of individual model coefficients were verified using analysis of variance (ANOVA), lack of fit test and sum of squares sequential model.

$$y' = \frac{1}{\sqrt{y+k}} \tag{3}$$

$$\frac{1}{\sqrt{R_a}} = 0.97942 - 0.012322A + 0.10833B - 0.18335C + \left(9.14658\times10^{-4}\right)AC + \left(1.90348\times10^{-4}\right)A^2 + \left(8.25823\times10^{-3}\right)C^2 \tag{4}$$

where A, B and C are rake angle in degree, nose radius in nm and feed rate in mm/min while R_a is the surface roughness in nm.

Figure 8 Box-cox plot for model transformation (see online version for colours)

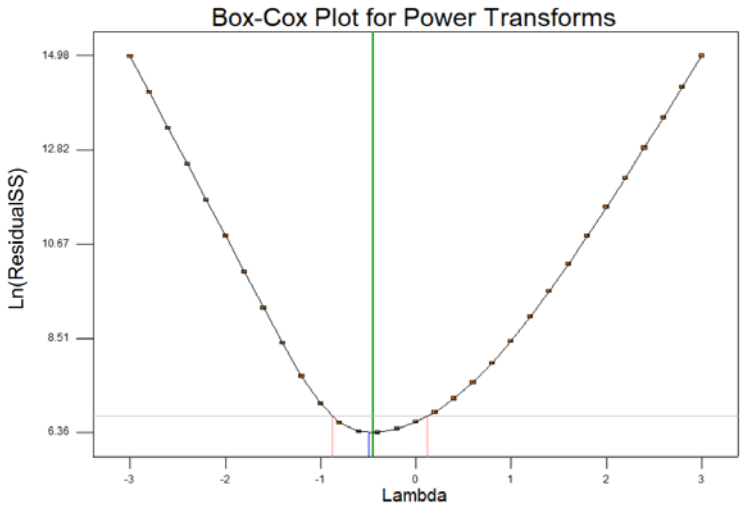

ANOVA is a standard statistical technique used to determine independent variable significance on output responses (Bouzid et al., 2014) by determining factor contributions in percentage on variability (variance). ANOVA table is made up of the *SS* (sum of squares), *df* (degrees of freedom), Mean Square (*MS*), F-value, % Contribution and p-values (Meddour et al., 2015). *SS* is employed in estimating the square of the deviation from the average, *MS* is the ratio between *SS* and *df*, F-value which requires the that

F-calculated be higher than that from F-table is the ratio of MS_i (regression mean square) and MS_e (mean square error) while *% Cont*. (percentage contribution) is the ratio of SS_f (individual factor sum of square) and SS_T (total sum of square). The relating equations are expressed in equations (5)–(8) (Chabbi et al., 2017):

$$SS_f = \frac{N}{Nn_f}\sum_{i=0}^{Nn_f}\left(\overline{y}_i - \overline{y}\right)^2 \tag{5}$$

$$MS = \frac{SS_i}{df_i} \tag{6}$$

$$F_i = \frac{MS_i}{MS_e} \tag{7}$$

$$\%Cont = \frac{SS_f}{SS_T}\times 100 \tag{8}$$

where i is the average of responses, y_i average observed experimental response at f_i level, N total number of experiments, Nn_f level of each factor f and $\overline{y} = \frac{1}{N}\sum_{i=0}^{n} y_i$. Tables 3 illustrates the ANOVA result for surface roughness (Ra) for 95% confidence level showing values for *SS*, *MS*, *df* and *% cont*. of each model terms.

The Model F-value of 38.44 and very low probability value (p = 0.0001) implies the model is significant (Table 3). There is only a 0.01% chance that a "Model F-Value" this large could occur due to noise. Values of "Prob > F" less than 0.05 indicate model terms are significant. In this case B (nose radius), C (feed rate), AC (rake angle/feed rate), A^2 (power of rake angle), C^2 (power of feed rate) are significant model terms. Values greater than 0.10 indicate the model terms are not significant (Zhang and Zheng, 2009). Term A (rake angle) has p-value ("Prob > F") higher than 0.05 indicating its partial or low significance on the R_a model. However, since it's the only insignificant and a main term that supports hierarchy, further model reduction is therefore not required.

Table 3 ANOVA test showing model adequacy

Source	*Sum of squares*	*Df*	*Mean Square*	*F Value*	*P-value Prob > F*	*% Contn*	*Remark*
Model	*0.72*	*6*	*0.12*	*38.44*	*< 0.0001*		*Significant*
A-Rake angle	9.19E-03	1	9.19E-03	2.96	0.1159	*1.23%*	
B-Nose radius	0.023	1	0.023	7.57	0.0204	*3.07%*	
C-Feed rate	0.47	1	0.47	152.99	< 0.0001	*62.67%*	
AC	0.035	1	0.035	11.13	0.0075	*4.67%*	
A^2	0.021	1	0.021	6.72	0.0269	*2.8%*	
C^2	0.18	1	0.18	58.03	<0.0001	*24.0%*	
Residual	0.031	10	3.10E-03				
Lack of fit	0.031	6	5.17E-03				
Pure error	0	4	0				
Cor total	0.75	16					

The Sequential Model Sum of Squares, the Lack of Fit tests, the Statistical model summary and the quadratic model suggested are shown in Tables 4–6. The Lack of Fit is mandated to be insignificant (p-value > 0.05) (Stat-Ease Inc USA, 2008). However, the p-value was not displayed in Lack of Fit Table (Table 5) because it requires that response values are available at replicated values of the model effects (https://www.jmp.com/support/help/14/lack-of-fit.shtml). The test involves computing an estimate of pure error, based on a sum of squares, using these replicated observations. Therefore, absence of Lack of Fit report means the test statistics cannot be computed because (https://www.jmp.com/support/help/14/lack-of-fit.shtml):

- There are no replicated points with respect to the X variables, so it is impossible to calculate a pure error sum of squares.
- The model is saturated, meaning that there are as many estimated parameters as there are observations. Such a model fits perfectly, so it is impossible to assess lack of fit.

Table 4 Sequential model sum of squares for surface roughness

Source	*Sum of squares*	*Df*	*Mean square*	*F Value*	*P-value Prob > F*	*Remark*
Mean vs Total	1.6	1	1.6			
Linear vs Mean	0.47	3	0.16	7.48	0.0037	
2FI vs Linear	0.04	3	0.013	0.57	0.6498	
Quadratic vs 2FI	*0.21*	*3*	*0.071*	*23.7*	*0.0005*	*Suggested*
Cubic vs Quadratic	0.021	3	6.99E-03	6.37E+07	< 0.0001	Aliased
Residual	0	4	0			
Total	2.35	17	0.14			

Table 5 Lack of fit tests for surface roughness

Source	*Sum of Squares*	*Df*	*Mean Square*	*F Value*	*P-value Prob > F*
Linear	0.27	9	0.03		
2FI	0.23	6	0.039		
Quadratic	0.021	3	6.99E-03		
Cubic	0	0			
Pure Error	0	4	0		

Table 6 Statistical model summary

Source	*Std. Dev*	*R-Squared*	*Adjusted R-Squared*	*Predicted R-Squared*	*PRESS*	*Remark*
Linear	0.15	0.6333	0.5487	0.329	0.5	
2FI	0.15	0.6865	0.4984	–0.2317	0.92	
Quadratic	0.055	0.9719	0.9358	0.5489	0.34	Suggested
Cubic	0	1	1	+	Aliased	

Tables 4–6 showed an aliased cubic model, this means that the effects of each variable that caused different signals become indistinguishable. Aside the cubic model which has the highest values of adjusted-R^2 (Adj-R^2) and predicted-R^2 (Pred- R^2) but aliased, the quadratic model becomes the next in choice (Table 6). In choosing a model, preference is given to that which maximises both Adj-R^2 and Pred-R^2 (Stat-Ease Inc USA, 2008). The percentage of contribution column in Table 7 (% Cont.) is a function of the sum of squares of the significant items considered. It is the portion reflecting what each significant factor and/or interaction contributes to the total variation observed in the experiment and it indicates the relative power of a factor to reduce the variation. Precise control of a factor level means that its effect would reduce/increase the total variation by the amount indicated by its percentage contribution.

Table 7 Summary of regression coefficient (R^2)

Std. Dev	*0.056*	R^2	*0.9584*
Mean	0.31	Adj-R^2	0.9335
C.V. %	18.16	Pred-R^2	0.8540
PRESS	0.11	Adeq Precision	18.954

As can be seen from Tables 7, the "Pred-R^2" of 0.8540 for the suggested quadratic model is close and in reasonable agreement with the "Adj-R^2" of 0.9358. Adj-R^2 is also required to be greater or equal to 0.70 for adequacy and accuracy of a models (Alao and Konneh, 2012). Thus, Adj-R^2 of 0.9335 indicate that the model is very significant. Furthermore, "Adeq Precision" is a measure of the signal to noise ratio where a ratio greater than 4 is desirable. Hence, the ratio of 18.954 indicates an adequate signal. In addition, a relatively lower value of the coefficient of variation (C.V = 18.16) indicates improved precision and reliability of the conducted experiments. Coefficient of determination (R^2), a ratio of the explained variation to the total variation measures the degree of fit (Burton and Kurien, 1959). However, a good model fit should yield an R^2 of at least 0.80 (Joglekar and May, 1987). Therefore, the response model with R^2 of 0.9584 and Adj-R^2 of 0.9335 at a confidence level of 95% as shown in Table 7 would explain the factor behaviour on the response very well.

Normality assumption plot i.e., Figure 9 (Normal Plot of Residuals) and Figure 10 (plot of Residuals vs. Predicted) were used to check the residuals to determine how well the model satisfies the assumptions of ANOVA. Also, the internally studentised residuals was used to measure the standard deviations separating the experimental and predicted values (Liu and Chiou, 2005). The straight line in Figure 9 showed that the residuals are falling on the straight line, which means the errors are distributed normally while Figure 10 indicated that the model possesses adequate normality of residuals and no constant error (Kumar et al., 2007). Therefore, the constant variance/independent assumption is not violated (Saleem and Somá, 2015).

3.2 Effects of factors on R_a

A look at Table 2 showed that by comparing Expt. runs: 9 & 12; 4 & 7; 14 & 15; 5 & 11 in which rake angle is increased as against other factors, it is evident that as the negative rake angle of tool increases, workpiece surface roughness reduces. This behaviour can be said to be caused by increase in ploughing due to chip and uncut chip thickness

compression that occurred ahead the cutting tool. From Expt. runs: 4 & 9; 10 & 17; 1 & 16; 7 & 12, it can as well be seen that high nose radius also seemed better regarding roughness reduction than low nose radius value. In nanomachining, the undeformed chip thickness is required (i.e., depth of cut) to be smaller than the edge radius, this is because, ductile cutting of brittle material (e.g. silicon) needs high compressive stress at the chip formation zone to stop pre-existing flaws growth. This reduction which can be achieved by nose radius increase, is responsible for the improvement of surface roughness seen in the compared runs. It was also documented that, the higher the difference between the radius and uncut chip thickness, the better the surface roughness in terms of measured peak to valley (Tauhiduzzaman and Veldhuis, 2014). Therefore, it is believed that the increase in nose radius caused a decrease in chip thickness which in turn made the thrust force to increase. This led to high compressive pressure in the cutting zone and an increase in materials volume undergoing this stress.

Figure 9 Normal probability plot of residuals in surface roughness modelling (see online version for colours)

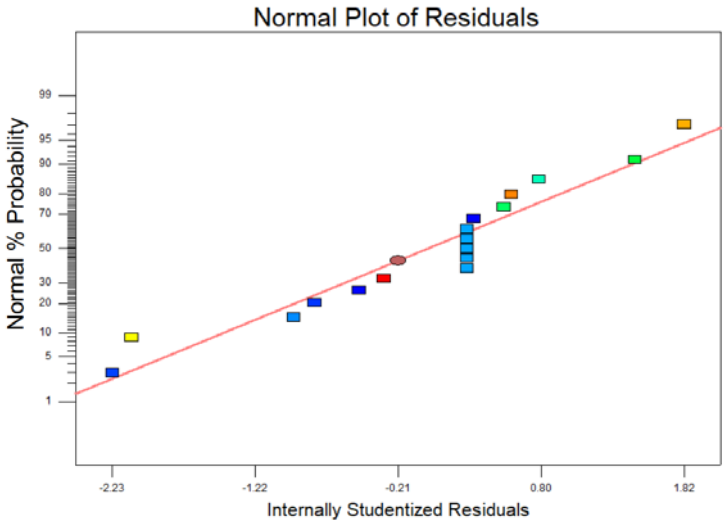

According to Liu et al. (2004), high nose radius is tantamount to increasing the ratio of thrust force to cutting force and that of thrust force to feed rate force. It also causes reduced residual diamond tool marks (i.e., continuous circular arcs imprints) on silicon thereby lowering the roughness (R_a) of the of the workpiece. The large negative effective rake angle created by the increase in edge roundness (nose radius) also further presses the materials in front of the cutting edge down in a compressive stress state and uniform stress field in the cutting region. Judging from the outputs of Expt. runs: 5 & 15; 10 & 16; 1 & 17; 11 & 14, it is evident that, low feed rate is better for surface roughness improvement than high feed rate. This is because the energy needed for crack propagation is higher than that needed for plastic yielding when the feed rate is small. The low plastic yielding as compared the high crack propagation energy is believed to account for the ease of brittle-ductile transition. The improvement seen with low feed rate was also noted by Cheng et al. (2014) is his work while considering feed rate, cutting speed and depth of cut as factors. The observed trend has further affirmed that changes in

feed rate is a strong determinant of variation in surface quality. The smoother surface with low feed rate as against high feed rate was due to increase in brittle fracture occurrence at high feed rate owing to high material removal rate (MRR). The behaviour of all the three process parameters represented using perturbation plot is shown in Figure 11.

Figure 10 Probability plot of residuals vs. predicted in surface roughness modelling (see online version for colours)

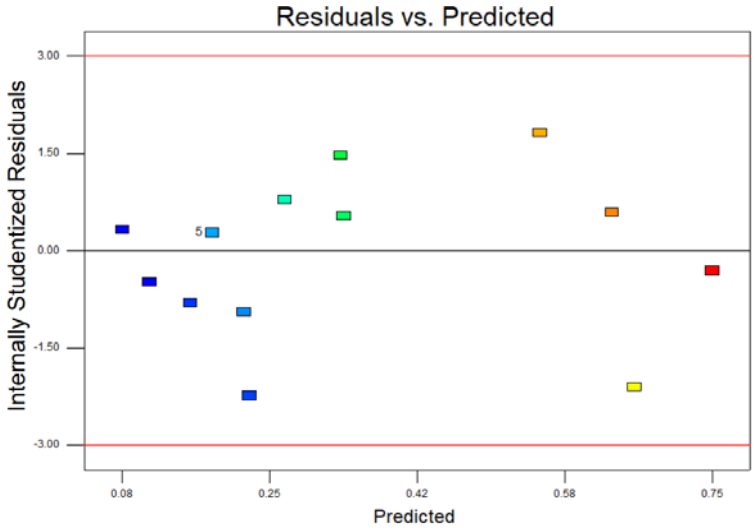

Figure 11 Perturbation plot comparing the effect of all considered factors at their mid-points in the design space

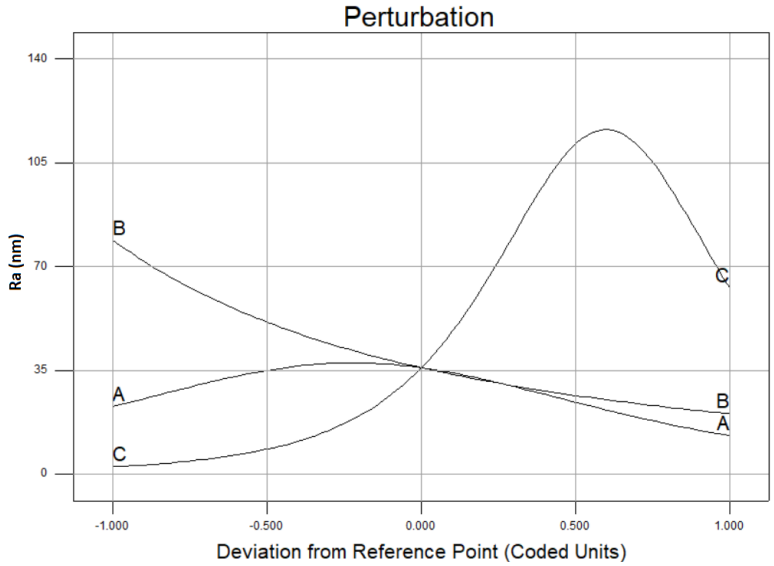

Figures 12 and 13 showed the influence of rake angle and nose radius at low and high feed rates. The figures stressed the dominance of feed rate over rake angle and nose

radius effects respectively. Increase in rake angle at low feed rate was observed to result in increased optical silicon surface roughness while nose radius has little effect at this level. In Figure 13, at 0° clearance angle, there was a profound difference in the behaviour of both low and high nose radius values. While low nose radius had negative influence on roughness, high nose radius had a positive influence. Meanwhile at high negative rake angle value as seen in this same graph, both low and high nose radius behaved alike, meaning that at low feed rate and high tool negativity, the influence of nose radius increase on silicon roughness seems to be lost. This might be due to increased compressive stress brought about by increasing tool negativity. The compressive stress increase also facilitated plastic removal at the cutting plane thereby overshadowing the nose radius effect.

Figure 12 Variation of R_a at 2 mm/min feed rate (see online version for colours)

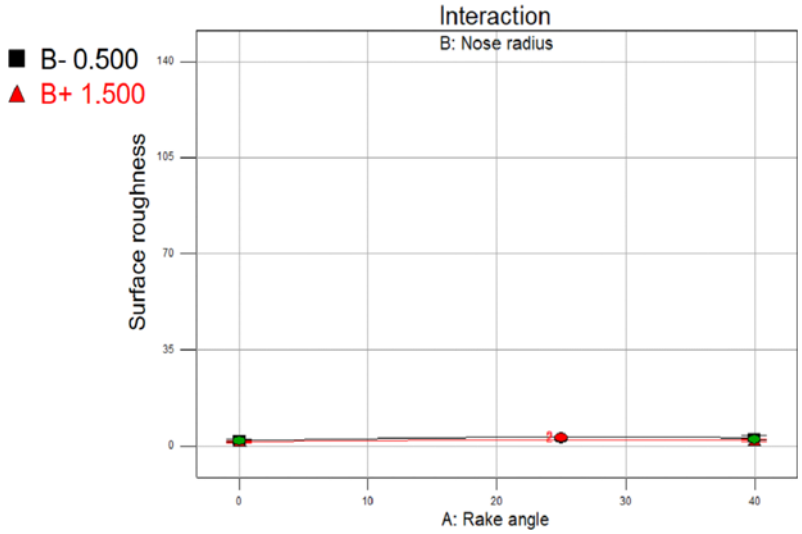

Figure 13 Variation of R_a at 12 mm/min feed rate (see online version for colours)

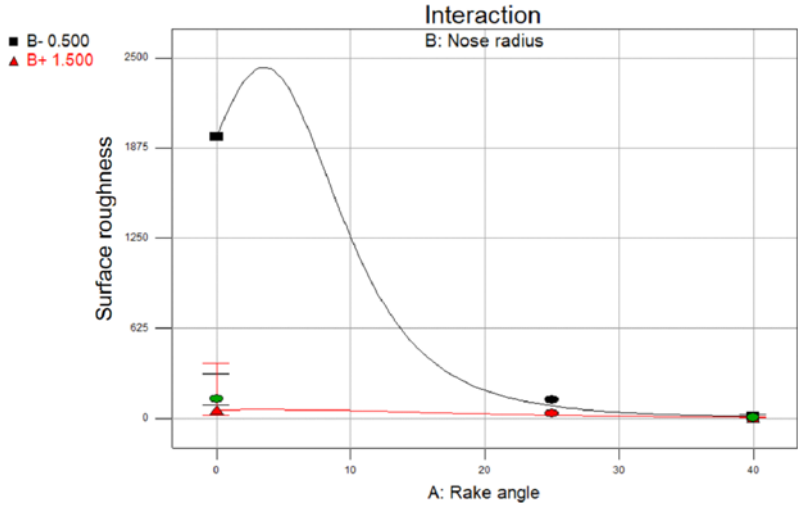

It was noted from this study that the larger the nose radius at lower feed rates is, the smoother the surface finish of the machined surface becomes. Although an increase in nose radius improved surface quality, its effect seems not felt at combined situations of high feed rate and high negative rake (Figures 13 and 14). This is believed to be due to negligible increase in compressive pressure in the cutting zone brought about by negligible increase in both radial cutting and thrust forces and negligible decrease in chip thickness. The increase in cutting and thrust forces brought about by large nose radius are known to cause decrease in effective depth, deep subsurface damage layer and high dimensional error (Yan et al., 2009; Yan et al., 2009). This observation is in agreement with the discovery of Tauhiduzzaman and Veldhuis who said nose radius influence seizes below a limiting value of feed rate (Tauhiduzzaman and Veldhuis, 2014). They obviously did not note that it also seizes above some limiting value of negative tool rake angle too.

Figure 14 Variation of R_a at rake angle 40° and feed rate 12 mm/min (see online version for colours)

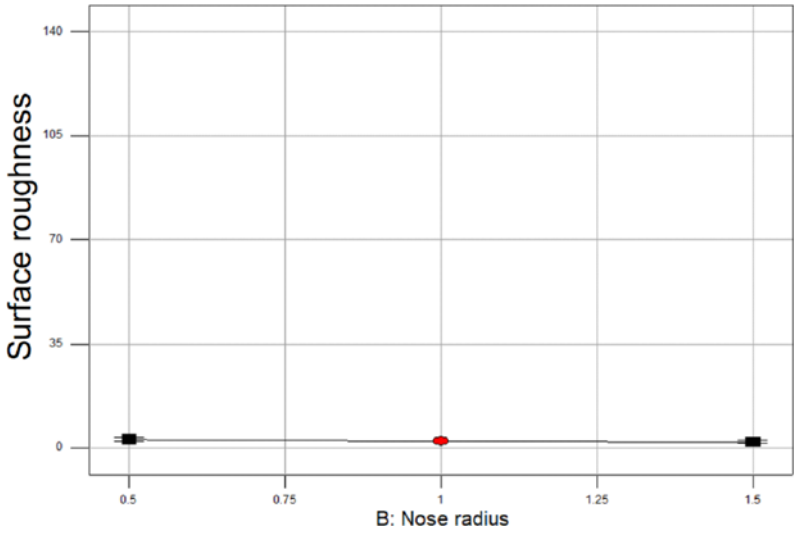

The interactive effect of feed rate and rake angle as observed from Figures 15 further iterated that both low feed rate and high negative rake angle improves surface quality. This also meant that high force caused by increase in feed rate at constant depth of cut and cutting speed (Otieno and Abou-El-Hossein, 2018; Abdulkadir and Abou-El-Hossein, 2018) is minimised as rake angle negativity increases since high negative rake angle ensures adequate hydrostatic pressure needed to causes plastic deformation under the tool (Zhou et al., 2001; Abdulkadir et al., 2019). Additionally, the increase in rake angle negativity led to increase in rubbing action at the tool-workpiece interface which was responsible for the temperature increase in the cutting region. It can then be deduced from the interactive effect that as both negative rake angle and feed rate increased, the machining condition improved creating a smoother workpiece surface. Further analysis of the experimental result considering Figures 16 and 17 showed that, high tool negativity led to surface roughness reduction while high feed rate resulted in poor roughness when machining at high negative rake angle, nose radius and feed rate. However, at low tool negativity, high nose radius also reduced the poor roughness caused by high feed rate

(i.e., roughness reduced from ~1700 nm at 0° rake angle, 0.5 mm nose radius and 12 mm/min feed rate to ~170 nm at 0° rake angle, 1 mm nose radius and 12 mm/min feed rate).

Figure 15 3D surface interactive effect plot of feed rate and rake angle on R_a at 1.5 mm nose radius (see online version for colours)

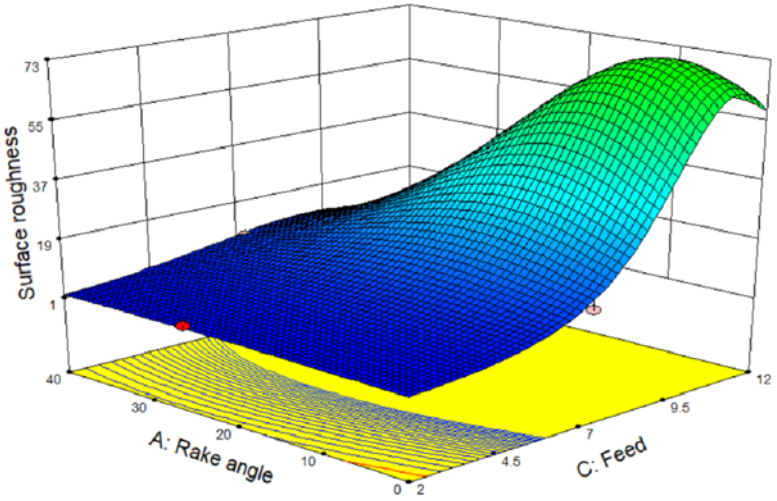

Figure 16 3D surface interactive effect plot of feed rate and rake angle on R_a at 0.5 mm nose radius (see online version for colours)

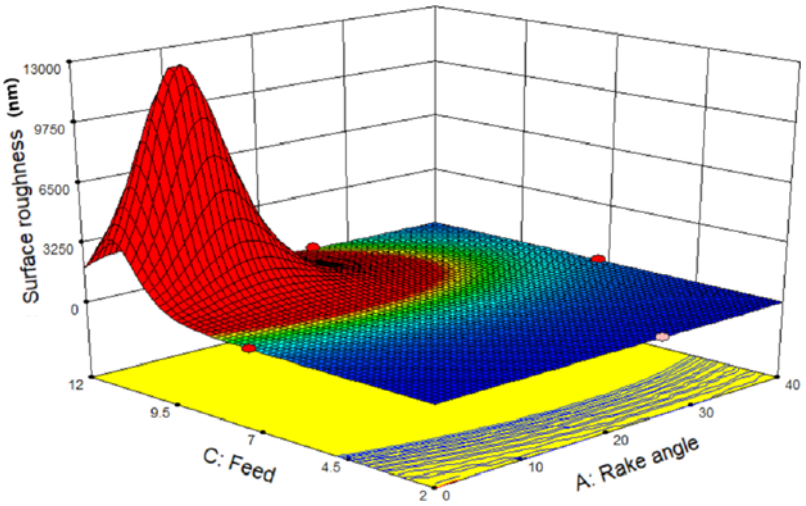

The observed better surface roughness at the lowest tool rake (i.e., 0°) could be due to the established fact that total von Misses strain, effective stress and main cutting force reduces with reduction in tool rake negativity (i.e., rake angle increase in positive direction) (Abdulkadir and Abou-El-Hossein, 2018, 2019). Literatures has it that, as the

negative rake angle gets larger, the machining condition also gets better (Sharma et al., 2013; Neo et al., 2012; Nakasuji et al., 1990; Tanaka et al., 2007). Therefore, the 1 mm nose radius used with 0° rake angle tool at 2 mm/min seem to be a good trio combination that enhanced high and deep layer formation of amorphous silicon at the machined region.

Figure 17 3D surface interactive effect plot of feed rate and rake angle on R_a at 1 mm nose radius (see online version for colours)

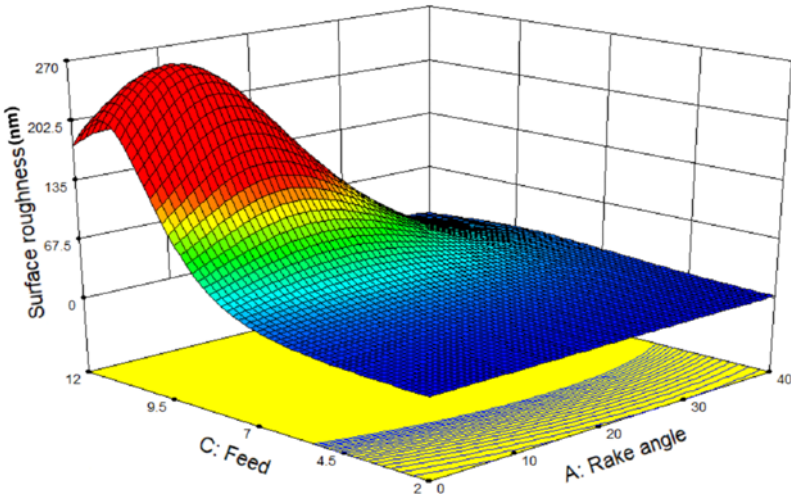

Additionally, improved R_a with high negative rake angle as observed in Figures 15 and 18 showed that, high negative rake angle suppresses fracture, increases compressive stresses and nullifies critical tool feed rate effect at cutting plane. Therefore, high rake angle reduced R_a at low and high nose radius than at a low rake angle value. However, the effect of rake angle on R_a was not felt when the feed rate was low, this meant that, 0° rake angle had the same effect as 40° rake angle when the feed rate was low, whether the nose radius is high or low (Figures 12 and 15). High negative rake angle was also observed to have a dominating effect at low and high nose radius on high feed rate, thereby increasing R_a as proven from literature (Yan et al., 2002; Neo et al., 2012) (Figures 13, 15 and 18. This meant that at low nose radius and tool negativity, high feed rate caused more surface damage than at high nose radius and tool negativity. This can be linked to the high edge roundness created due to high effective negative rake angle and nose radius. High edge roundness is known to suppress materials ahead the cutting edge which could be the reason responsible for silicon plastic removal during ultra-precision diamond turning (Abou-El-Hossein, 2013; Blake and Scattergood, 1990; Leung et al., 1998; Zhang et al., 2015). The improvement in the surface quality as noticed can also be due to negative rake angle tool's stronger cutting edge which enhanced workpiece material ductile behaviour as stated by (Blackley and Scattergood, 1991; Leung et al., 1998; Patten and Gao, 2001; Yan et al., 2001).

Figure 18 Feed rate and rake angle effect on R_a at 1.5 mm nose radius (see online version for colours)

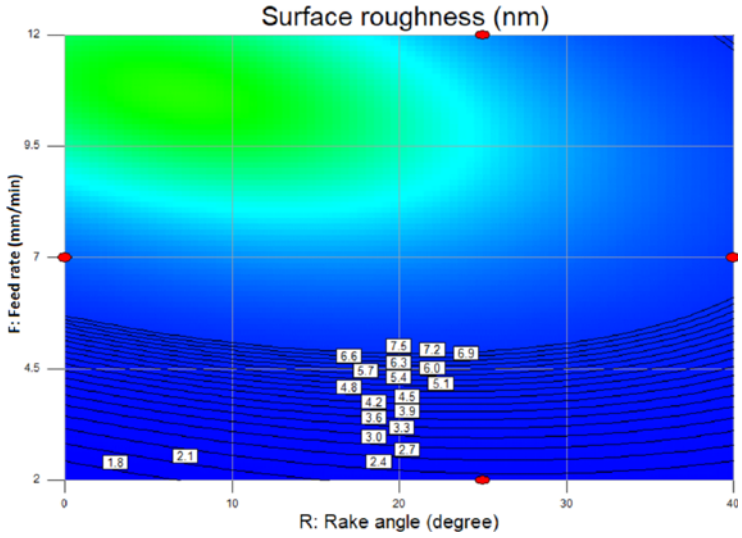

4 Optimisation of surface roughness

Optimisation is the process of improving analytical process performance in order to obtain the best response (Candioti et al., 2014). Optimisation of R_a involved searching for best combinations of factor levels which simultaneously satisfies the intended goal of a minimised roughness. Of the different optimisation approaches, composite desirability based on weighted geometric mean of the individual response desirability on a zero to one range is most widely used (Dikshit et al., 2016). The goals form a desirability function which is sought from random to steepest slope and finally to a maximum (Stat-Ease Inc USA, 2008). However, two or more optimum values may exist due to curvature in response surfaces and their combinations in desirability function.

4.1 Setting optimisation criteria

The optimisation approach used in this study is termed "Desirability function approach". This involved transforming the measured properties of each predicted response into a dimensionless desirability value, D, with a scale of between D (i.e., $d_i(\hat{y}_i)) = 0$ (undesirable response) and D (i.e., $d_i(\hat{y}_i)) = 1$ (desirable/ideal response) (Hazir et al., 2018; Chabbi et al., 2017; Candioti et al., 2014; Sahoo and Mishra, 2014). The desirability function technique provides different solutions from which the highly desirable can be chosen (Sahoo and Mishra, 2014). The technique is widely used for parameter optimisation (Palanikumar et al., 2008). Depending on the intended optimisation criteria, different functions within the acceptable response range of values given by $(U_i–L_i)$ are employed (Candioti et al., 2014). To maximise (equations (9)), minimise (equations (10)) or set a target value T_i as most desirable response (equations (11)), requires the following equations:

$$d_i\left(\hat{y}_i\left(x\right)\right)=\begin{bmatrix}0 & if\ \hat{y}_i\left(x\right)<L_i\\ \left(\dfrac{\hat{y}_i\left(x\right)-L_i}{U_i-L_i}\right)^s & if\ L_i\le\hat{y}_i\left(x\right)\le U_i\\ 1 & if\ \hat{y}_i\left(x\right)>L_i\end{bmatrix} \tag{9}$$

$$d_i\left(\hat{y}_i\left(x\right)\right)=\begin{bmatrix}1 & if\ \hat{y}_i\left(x\right)<L_i\\ \left(\dfrac{U_i-\hat{y}_i\left(x\right)}{U_i-L_i}\right)^t & if\ L_i\le\hat{y}_i\left(x\right)\le U_i\\ 0 & if\ \hat{y}_i\left(x\right)>L_i\end{bmatrix} \tag{10}$$

$$d_i\left(\hat{y}_i\left(x\right)\right)=\begin{bmatrix}0 & if\ \hat{y}_i\left(x\right)<L_i\\ \left(\dfrac{\hat{y}_i\left(x\right)-L_i}{T_i-L_i}\right)^s & if\ L_i<\hat{y}_i\left(x\right)<T_i\\ 1 & \hat{y}_i\left(x\right)=T_i\\ \left(\dfrac{\hat{y}_i\left(x\right)-U_i}{T_i-U_i}\right)^t & if\ T_i<\hat{y}_i\left(x\right)<U_i\\ 0 & if\ \hat{y}_i\left(x\right)>U_i\end{bmatrix} \tag{11}$$

where $d_i(\hat{y}_i)$ is the desirability function, $\hat{y}_i\left(x\right)$ is the individual response, U_i is the response acceptable upper value, L_i is the response acceptable lower value, s is the weight i.e., power value determining the importance of $\hat{y}_i$ to be close to maximum, t is the weight i.e., power value determining the importance of $\hat{y}_i$ to be close to minimum, T_i is the target value.

The criteria for the module goal was set to "*in range"* for all the factors to span the experimental levels of the three chosen factors and prevent extrapolation (Chabbi et al., 2017). To get the best combinations that minimises the response, the goal for the response (surface roughness) was set to "*minimise"***.** The simultaneous objective function for optimisation is a geometric mean of transformed responses and is given in equations 12 and 13 as:

$$D=\left(d_1\times d_2\times\cdots\times d_n\right)^{1/n}=\left(\prod_{i=1}^{n}d_i\right)^{1/n} \tag{12}$$

$$F\left(x\right)=-D \tag{13}$$

Each response is required to have both low and high value assigned to each goal for simultaneous optimisation. The desirability is then defined by equation (14) when searching for minimum response value (Chabbi et al., 2017):

$$\begin{cases} d_i = 1 & \text{if response} < \text{low value} \\ 1 \geq d_i \geq 0 & \text{as response varies from low to high} \\ d_i = 0 & \text{if response} > \text{high value} \end{cases} \quad (14)$$

4.2 Analyses of optimised solution

In the process of finding an optimised combination, thirty-six (36) solutions (Table 8) were chosen out of forty-three (43) list of the random search starting points. Table 8 can be considered in two optimisation approaches termed "Quality optimisation and Productivity optimisation". In quality optimisation, minimum surface roughness (R_a) value was considered (i.e., S/N 1 to 26) while in productivity optimisation, maximum material removal rate (MRR) was considered using high machining feed rate (i.e., S/N 27 to 36).

Table 8 Desirable factor combinations

S/N	*Rake angle (^{0})*	*Nose radius (mm)*	*Feed rate (μm/rev)*	*Surface roughness (nm)*	*Desirability*	*Remark*
1	0	1	2	1.75851	1	
2	*1.0733*	*1.49708*	*2.00747*	*1.57908*	*1*	*Selected*
3	0.267756	1.47347	2.15975	1.6486	1	
4	0.292916	1.01939	2.04873	1.79763	1	
5	0.520777	1.27556	2.1713	1.76312	1	
6	3.75759	1.31662	2.01543	1.78066	1	
7	0.0711087	1.086	2.09496	1.78503	1	
8	0.558215	1.33087	2.05623	1.66174	1	
9	5.43033	1.48209	2.03048	1.77524	1	
10	0.0467024	0.945721	2.00147	1.78966	1	
11	0.118092	1.3322	2.15623	1.70614	1	
12	2.28E-05	0.857593	2	1.83274	0.99	
13	3.58E-06	0.783534	2	1.87321	0.978	
14	11.5944	1.5	2	1.97153	0.95	
15	39.9999	1.49588	2	2.08425	0.92	
16	39.9017	1.49999	2	2.08436	0.92	
17	39.9999	1.45962	2	2.10809	0.914	
18	38.3043	1.5	2.00001	2.12725	0.909	
19	37.742	1.49999	2.00001	2.14122	0.906	
20	35.3808	1.5	2	2.19282	0.894	
21	34.6558	1.49999	2.00055	2.20668	0.891	
22	24.7026	1.5	2	2.2598	0.878	
23	29.83	1.5	2	2.26371	0.878	

Table 8 Desirable factor combinations (continued)

S/N	*Rake angle (^{0})*	*Nose radius (mm)*	*Feed rate (µm/rev)*	*Surface roughness (nm)*	*Desirability*	*Remark*
24	29.577	1.5	2.00263	2.26733	0.877	
25	5.24658	0.5	2.00001	2.366	0.856	
26	39.9997	0.816341	2.00001	2.60945	0.808	
27	*40*	*1.5*	*12*	*6.86469*	*0.448*	*Selected*
28	39.648	1.5	12	7.04299	0.441	
29	40	1.5	11.8927	7.06411	0.44	
30	40	1.44355	12	7.09005	0.439	
31	39.45	1.5	12	7.1456	0.437	
32	39.9999	1.24845	12	7.96098	0.407	
33	40	1.49962	11.2472	8.27692	0.397	
34	40	1.09196	12	8.78081	0.381	
35	4.00E+01	0.971744	12	9.49988	0.362	
36	1.31E-05	1.5	11.7499	61.2658	0.063	

Of these solutions, serial number 2 gave the lowest R_a value (1.57908 nm) while serial number 27 gave a good result when productivity optimisation is required (i.e., least roughness at maximum feed rate). A Ramps desirability view, Bar graph, contour and 3D surface desirability graphs of quality optimisation factors and responses are displayed in Figures 19–22.

Figure 19 Ramps desirability view (see online version for colours)

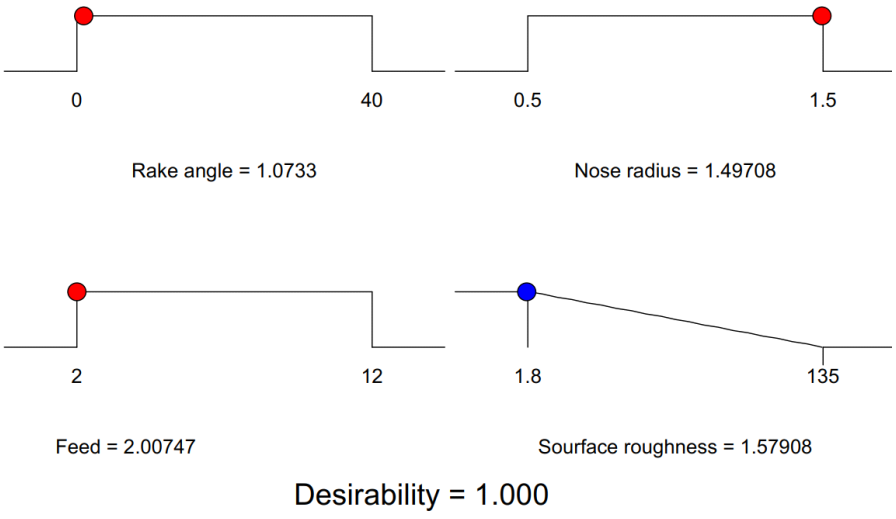

Figure 20 Desirability bar graph (see online version for colours)

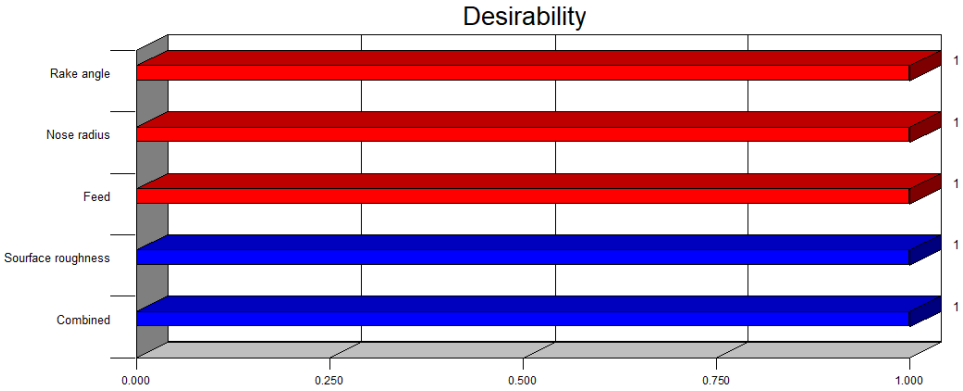

Figure 21 Desirability contour plot (see online version for colours)

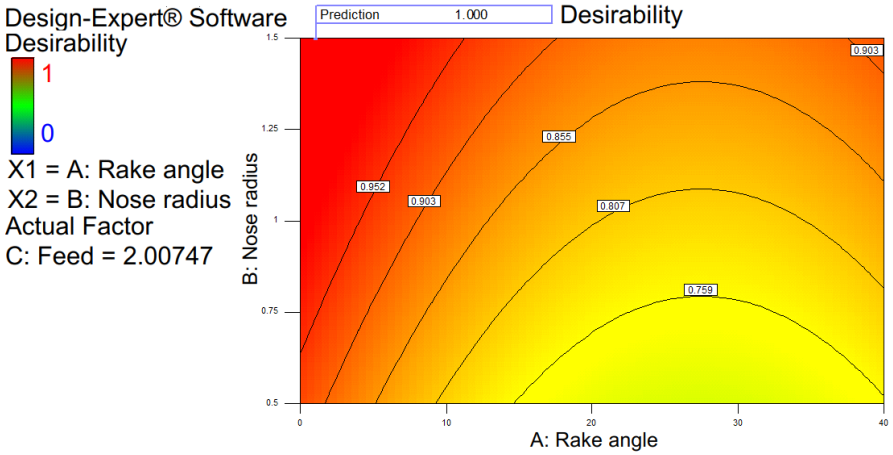

Figure 22 3D surface desirability plot (see online version for colours)

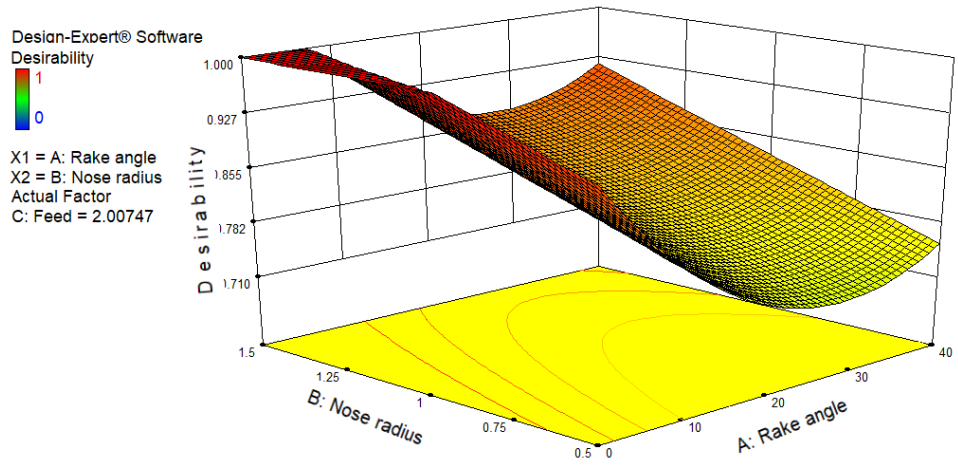

The Ramps view (Figure 19) displayed factors and response desirability by red and blue colours. The red coloured points indicate the desired factor levels while the blue points show how well the goal is satisfied. The higher up the ramp the better. Looking at both the contour and the 3D Surface plots, it is evident that desirability increases throughout with increased nose radius while it decreased and later increased with higher rake angle values. However, the optimised factor combinations gave a slightly lower R_a (1.57908 nm) than the experimentally measured R_a (1.8 nm). To validate the optimised output values, the optimal desirability function machining parameter values were substituted in the transformed regression model given in equation 12 where A is rake angle optimal solution, B is the optimal solution of nose radius, C an optimal solution of feed rate, and R_a an optimal solution of the surface roughness. The computed function results are shown by equations 13 and 14.

$$R_a = [(0.97942 - 0.012322A + 0.10833B - 0.18335C + \left(9.14658\times10^{-4}\right)AC + \left(1.90348\times10^{-4}\right)A^2 + \left(8.25823\times10^{-3}\right)C^2]^{-2} \quad (12)$$

$$R_a = [(0.97942 - 0.012322\left(1.0733\right) + 0.10833(.49708) - 0.18335(2.00747) + \left(9.14658\times10^{-4}\right)(1.0733\times2.00747) + \left(1.90348\times10^{-4}\right)\left(1.0733\right)^2 + \left(8.25823\times10^{-3}\right)\left(2.00747\right)^2]^{-2} \quad (13)$$

$$R_a = 1.579139544 \text{ nm} \quad (14)$$

The transformed optimal processing parameter values using the model equation gave roughness (R_a) value of 1.579139544 nm which quite agreed with the desirability function value of 1.57908 nm for the objective function R_a as shown in Table 8. This optimisation study has successfully examined optimisation based on quality and production rate (productivity). As evident from Table 8, solutions 1 – 26 are desirable when the set goal is for quality manufacturing (low R_a). This is because, these solutions require machining at low feed rate range of between 2–~2.2 μm/rev. However, machining at a speed this low is best suited for finish cuts. On the other hand, solutions 27– 36 have high feed rates ranging from ~11.3 – 12 μm/rev. Machining at feed rate this high will boost production rate at the detriment of product quality.

5 Conclusion

Design of experiment optimisation approach was employed in finding effective variables and their optimal levels that can minimise R_a when ultra-high precision diamond turning a monocrystalline optical grade silicon using water as coolant. Three factors (i.e., machining parameters: rake angle, nose radius and feed rate) at three levels were selected with clearance angle, depth of cut and cutting speed kept constant. The highly effective interactions and main variable effects of the processing factors were determined using BBD approach and the following conclusions drawn from the analysis of the results:

1 Backward elimination regression analysis method was used in eliminating the non-significant factors to arrive at an appropriate mathematical model.

2 The high R2 and R2-adjusted values (95.84% and 93.35%) authenticated the significance of the machining parameters and the validity of regression equation to adequately predict roughness while the ANOVA and normal probability plots of the residuals and residuals versus predicted response also showed normal errors distribution with no unusual structure and pattern, implying that the model is good for prediction.

3 ANOVA analysis demonstrated that feed rate has significant effect on surface roughness with a percentage contribution of 62.67% while rake angle contributed the least amount (1.23%).

4 During the experiment, 1.8 nm surface finish which is less than the optically required 8 nm was attained at optimum machining conditions of 0° rake angle, 2 mm/min feed rate and 1.0 mm nose radius.

5 Desirability function approach was applied to optimise the cutting parameters and the optimal parametric setting obtained was verified using the model equation. The model equation was found to accurately predict the surface roughness given at optimised cutting parameters.

6 It was deduced from the study that machining condition improves with smoother surfaces as the nose radius and negative rake angle increases with reduction in feed rate.

7 It was observed from the result that the improvement in R_a due to increase in nose radius diminishes greatly at low feed rate and high negative rake cutting conditions.

8 An interesting observation made from this study which have not been reported in literature is that: as the tool negative rake angle value increases at high nose radius, the known poor roughness of machined surface caused by high feed rate reduced and overshadowed.

9 Additionally, as the tool nose radius increases at 0° rake angle, negative influence (i.e., increase roughness) of high feed rate on surface quality also reduces. These interesting effects of negative rake angle and nose radius increase on high feed rate would be beneficial for mass production where production rate boost is required with product quality maintained as shown in the optimisation result.

Acknowledgement

This is to acknowledge the intervention of Research Capacity Development of Nelson Mandela University (RCD) for the providing necessary fund to enable the completion of this research (RCD NMU No: s215102134). Our sincere appreciation also goes to Prof. Khaled Habou-El-Hossien for the guidance and support in carrying out this study. Worthy of mentioning is the South African Center for High Performance Computing for the use of both Material Studio software and cluster. We are particularly grateful to Dr. Krishna K. Govender for his tireless attention when called upon.

References

Abdulkadir, L.N. and Abou-El-Hossein, K. (2018) 'Observed edge radius behavior during MD nanomachining of silicon at a high uncut chip thickness', *The International Journal of Advanced Manufacturing Technology*, Vol. 101, Nos. 5–8, pp.1741–1757.

Abdulkadir, L.N. and Abou-El-Hossein, K. (2019) 'Diamond tool wear mode, path and tip temperature distribution considering effect of varying rake angle and Duncut/Redge ratio', *Surface Topography: Metrology and Properties*, Vol. 7, No. 2, pp.1–15.

Abdulkadir, L.N., Abou-El-Hossein, K., Abioye, A.M., Liman, M.M., Cheng, Y-C. and Abbas, A.A. (2019) 'Process parameter selection for optical silicon considering both experimental and AE results using Taguchi L9 orthogonal design', *The International Journal of Advanced Manufacturing Technology*, Vol. 103, Nos. 9–12, pp.4355–4367.

Abdulkadir, L.N., Abou-El-Hossein, K., Jumare, A.I., Liman, M.M., Olaniyan, T.A. and Odedeyi, P.B. (2018) 'Review of molecular dynamics/experimental study of diamond-silicon behavior in nanoscale machining', *The International Journal of Advanced Manufacturing Technology*, Vol. 98, Nos. 1–4, pp.317–371.

Abdulkadir, L.N., Abou-El-Hossein, K., Jumare, A.I., Odedeyi, P.B., Liman, M.M. and Olaniyan, T.A. (2018) 'Ultra-precision diamond turning of optical silicon–a review', *The International Journal of Advanced Manufacturing Technology*, Vol. 96, Nos. 1–4, pp.173–208.

Abdulkadir, L.N., Abou-El-Hossein, K., Liman, M.M., Babatunde, O.P. and Jumare, A.I. (2019) 'Molecular dynamic study of combined effects of diamond tool rake angle and duncut/Redge ratio on nanomachining behaviour of monocrystalline optical silicon', *International Journal of Computational Materials Science and Surface Engineering*, Vol. 8, Nos. 3–4, pp.245–268.

Abou-El-Hossein, K. (2013) 'Quality of silicon convex lenses fabricated by ultra-high precision diamond machining', *South African Journal of Industrial Engineering*, Vol. 24, No. 1, May, pp.91–97.

Alao, A-R. and Konneh, M. (2012) 'Surface finish prediction models for precision grinding of silicon', *The International Journal of Advanced Manufacturing Technology*, Vol. 58, Nos. 9–12, pp.949–967.

Asiltürk, I., Neşeli, S. and Ince, M.A. (2016) 'Optimisation of parameters affecting surface roughness of co28Cr6Mo medical material during CNC lathe machining by using the Taguchi and RSM methods', *Measurement*, Vol. 78, pp.120–128.

Ayomoh, M. and Abou-El-Hossein, K. (2015) 'Surface finish in ultra-precision diamond turning of single-crystal silicon', *SPIE Optifab*, p.96331I-96331I-6.

Blackley, W. and Scattergood, R.O. (1991) 'Ductile-regime machining model for diamond turning of brittle materials', *Precision Engineering*, Vol. 13, No. 2, pp.95–103.

Blake, P.N. and Scattergood, R.O. (1990) 'Ductile-Regime machining of germanium and silicon', *Journal of the American Ceramic Society*, Vol. 73, No. 4, pp.949–957.

Bouzid, L., Boutabba, S., Yallese, M.A., Belhadi, S. and Girardin, F. (2014) 'Simultaneous optimization of surface roughness and material removal rate for turning of X20Cr13 stainless steel', *The International Journal of Advanced Manufacturing Technology*, Vol. 74, No. 5, 1 September, pp.879–891.

Burton, M. and Kurien, K. (1959) 'Effects of solute concentration in radiolysis of water', *The Journal of Physical Chemistry*, Vol. 63, No. 6, pp.899–904.

Candioti, L.V., De Zan, M.M., Cámara, M.S. and Goicoechea, H.C. (2014) 'Experimental design and multiple response optimization using the desirability function in analytical methods development', *Talanta*, Vol. 124, pp.123–138.

Chabbi, A., Yallese, M.A., Meddour, I., Nouioua, M., Mabrouki, T. and Girardin, F. (2017) 'Predictive modeling and multi-response optimization of technological parameters in turning of polyoxymethylene polymer (POM C) using RSM and desirability function', *Measurement*, Vol. 95, pp.99–115.

Cheng, Y-C., Hsu, W-Y., Abou-El-Hossein, K., Olufayo, O. and Otieno, T. (2014) 'Investigation of diamond turning: of rapidly solidified aluminum alloys', *Current Developments in Lens Design and Optical Engineering* XV, p.919214.

Dean, A. and Voss, D. (1999) *Design and Analysis of Experiments* [Online resources], 11/11/2015.

Dikshit, M.K., Puri, A.B. and Maity, A. (2016) 'Empirical modelling of dynamic forces and parameter optimization using teaching-learning-based optimization algorithm and RSM in high speed ball-end milling', *Journal of Production Engineering*, Vol. 19, No. 1, pp.11–21.

Dogra, M., Sharma, V. and Dureja, J. (2011) 'Effect of tool geometry variation on finish turning-a. review', *Journal of Engineering Science and Technology Review*, Vol. 4, No. 1, pp.1–13.

Faehnle, O., Doetz, M. and Dambon, O. (2017) 'Analysis of critical process parameters of ductile mode grinding of brittle materials', *Advanced Optical Technologies*, Vol. 6, No. 5, pp.349–358.

Fang, F.Z. and Zhang, G.X. (2003) 'An experimental study of edge radius effect on cutting single crystal silicon', *The International Journal of Advanced Manufacturing Technology*, Vol. 22, No. 9–10, pp.703–707.

Ferreira, S.C., Bruns, R., Ferreira, H., Matos, G., David, J., Brandao, G., da Silva, E.P., Portugal, L.A., Dos Reis, P.S. and Souza, A.S. (2007) 'Box-behnken design: an alternative for the optimization of analytical methods', *Analytica Chimica Acta*, Vol. 597, No. 2, pp.179–186.

Fulemova, J. and Janda, Z. (2014) 'Influence of the cutting edge radius and the cutting edge preparation on tool life and cutting forces at inserts with wiper geometry', *Procedia Engineering*, Vol. 69, pp.565–573.

Hazir, E., Erdinler, E.S. and Koc, K.H. (2018) 'Optimization of CNC cutting parameters using design of experiment (DOE) and desirability function', *Journal of Forestry Research*, Vol. 29, No. 5, pp.1423–1434.

Hocheng, H. and Hsieh, M. (2004) 'Signal analysis of surface roughness in diamond turning of lens molds', *International Journal of Machine Tools and Manufacture*, Vol. 44, No. 15, pp.1607–1618.

Jacob, S. and Banerjee, R. (2016) 'Modeling and optimization of anaerobic codigestion of potato waste and aquatic weed by response surface methodology and artificial neural network coupled genetic algorithm', *Bioresource Technology*, Vol. 214, pp.386–395.

Jithin Babu, R. and Babu, A.R. (2014) 'Correlation among the cutting parameters, surface roughness and cutting forces in turning process by experimental studies', *Presented at the 5th International & 26th All India Manufacturing Technology, Design and Research Conference (AIMTDR 2014)*, IIT Guwahati, Assam, India.

Joglekar, A. and May, A. (1987) 'Product excellence through design of experiments', *Cereal Foods World*, Vol. 32, No. 12, p.857-&.

Jumare, A.I., Abou-El-Hossein, K. and Abdulkadir, L. (2017) 'Review of ultra-high precision diamond turning of silicon for infrared optics', *PONTE International Scientific Researchs Journal*, Vol. 73, No. 11, pp.58–123.

Jumare, A.I., Abou-El-Hossein, K., Goosen, W.E., Cheng, Y-C., Abdulkadir, L.N., Odedeyi, P.B. and Liman, M.M. (2018) 'Prediction model for single-point diamond tool-tip wear during machining of optical grade silicon', *The International Journal of Advanced Manufacturing Technology*, Vol. 98, Nos. 9–12, 11 July, pp.2519–2529.

Kandananond, K. (2009) 'Characterization of FDB sleeve surface roughness using the Taguchi approach', *European Journal of Scientific Research*, Vol. 33, No. 2, pp.330–337.

Kong, M., Lee, W., Cheung, C. and To, S. (2006) 'A study of materials swelling and recovery in single-point diamond turning of ductile materials', *Journal of Materials Processing Technology*, Vol. 180, No. 1, pp.210–215.

Krimpenis, A., Fountas, N., Ntalianis, I. and Vaxevanidis, N. (2014) 'CNC micromilling properties and optimization using genetic algorithms', *The International Journal of Advanced Manufacturing Technology*, Vol. 70, Nos. 1–4, pp.157–171.

Kumar, M.P., Ramakrishna, N., Amarnath, K., Kumar, M.S., Kumar, M.P., Ramakrishna, N., Amarnath, K. and Kumar, M.S. (2015) 'Study on tool life and its failure mechanisms', *International Journal for Innovative Research in Science and Technology*, Vol. 2, No. 04, pp.126–131.

Kumar, S., Kumar, P. and Shan, H. (2007) 'Effect of evaporative pattern casting process parameters on the surface roughness of Al–7% Si alloy castings', *Journal of Materials Processing Technology*, Vol. 182, Nos. 1–3, pp.615–623.

Lee, W., Cheung, B.C. (2003) *Surface Generation in Ultra-Precision Diamond Turning: Modelling, Practices*, Vol. 12, John Wiley & Sons, UK.

Leung, T., Lee, W. and Lu, X. (1998) 'Diamond turning of silicon substrates in ductile-regime', *Journal of Materials Processing Technology*, Vol. 73, No. 1, pp.42–48.

Leung, T.P., Lee, W.B. and Lu, X.M. (1998) 'Diamond turning of silicon substrates in ductile-regime', *Journal of Materials Processing Technology*, Vol. 73, No. 1, pp.42–48.

Liu, H-L. and Chiou, Y-R. (2005) 'Optimal decolorization efficiency of reactive red 239 by UV/TiO2 photocatalytic process coupled with response surface methodology', *Chemical Engineering Journal*, Vol. 112, Nos. 1–3, pp.173–179.

Liu, M., Takagi, J-I. and Tsukuda, A. (2004) 'Effect of tool nose radius and tool wear on residual stress distribution in hard turning of bearing steel', *Journal of Materials Processing Technology*, Vol. 150, No. 3, pp.234–241.

Luo, X., Goel, S. and Reuben, R.L. (2012) 'A quantitative assessment of nanometric machinability of major polytypes of single crystal silicon carbide', *Journal of the European Ceramic Society*, Vol. 32, No. 12, pp.3423–3434.

Meddour, I., Yallese, M., Khattabi, R., Elbah, M. and Boulanouar, L. (2015) 'Investigation and modeling of cutting forces and surface roughness when hard turning of AISI 52100 steel with mixed ceramic tool: cutting conditions optimization', *The International Journal of Advanced Manufacturing Technology*, Vol. 77, Nos. 5–8, pp.1387–1399.

Mukaida, M. and Yan, J. (2017) 'Ductile machining of single-crystal silicon for microlens arrays by ultraprecision diamond turning using a slow tool servo', *International Journal of Machine Tools and Manufacture*, Vol. 115, pp.2–14.

Nakasuji, T., Kodera, S., Hara, S., Matsunaga, H., Ikawa, N. and Shimada, S. (1990) 'Diamond turning of brittle materials for optical components', *CIRP Annals-Manufacturing Technology*, Vol. 39, No. 1, pp.89–92.

Neo, W.K., Kumar, A.S. and Rahman, M. (2012) 'A review on the current research trends in ductile regime machining', *The International Journal of Advanced Manufacturing Technology*, Vol. 63, No. 5, pp.465–480.

Otieno, T. and Abou-El-Hossein, K. (2018) 'Cutting forces and acoustic emission in the diamond turning of rapidly-solidified aluminium', *Insight-Non-Destructive Testing and Condition Monitoring*, Vol. 60, No. 1, pp.11–18.

Palanikumar, K., Muthukrishnan, N. and Hariprasad, K. (2008) 'Surface roughness parameters optimization in machining A356/SiC/20p metal matrix composites by PCD tool using response surface methodology and desirability function', *Machining Science and Technology*, Vol. 12, No. 4, pp.529–545.

Patten, J.A. and Gao, W. (2001) 'Extreme negative rake angle technique for single point diamond nano-cutting of silicon', *Precision Engineering*, Vol. 25, No. 2, pp.165–167.

Ravindra, D. and Patten, J. (2011) *Ductile Regime Material Removal of Silicon Carbide (SiC)*, Nova Science Publishers, Inc.

Rhorer, R.L. and Evans, C.J. (1995) 'Fabrication of optics by diamond turning', *Handbook of Optics*, Vol. 1, pp.41.1–41.3.

Sahoo, A. and Mishra, P. (2014) 'A response surface methodology and desirability approach for predictive modeling and optimization of cutting temperature in machining hardened steel', International *Journal of Industrial Engineering Computations*, Vol. 5, No. 3, pp.407–416.

Saleem, M. and Somá, A. (2015) 'Design of experiments based factorial design and response surface methodology for MEMS optimization', *Microsystem Technologies*, Vol. 21, No. 1, pp.263–276.

Sata, T. (2006) 'Surface finish in metal cutting', *CIRP ANN*, Vol. 12, No. 4, pp.190–197.

Sata, T., Li, M., Takata, S., Hiraoka, H., Li, C., Xing, X., Xing, X.Z. and Xiao, X.G. (1985) 'Analysis of surface roughness generation in turning operation and its applications', *CIRP Annals-Manufacturing Technology*, Vol. 34, No. 1, pp.473–476.

Sharma, K., Mahto, D. and Sen, S. (2013) 'In metal turning, effect of various parameters on cutting tool: a review', *International Journal of Application or Innovation in Engineering and Management (IJAIEM)*, Vol. 2, No. 8, August, pp.32–38.

Shibata, T., Fujii, S., Makino, E. and Ikeda, M. (1996) 'Ductile-regime turning mechanism of single-crystal silicon', *Precision Engineering*, Vol. 18, No. 2, pp.129–137.

Stat-Ease Inc USA (2008) *Design-Expert ® Version 7.1.6 Software*, ed, 2008.

Tanaka, H., Shimada, S. and Anthony, L. (2007) 'Requirements for ductile-mode machining based on deformation analysis of mono-crystalline silicon by molecular dynamics simulation', *CIRP Annals -Manufacturing Technology*, Vol. 56, No. 1, pp.53–56.

Tauhiduzzaman, M. and Veldhuis, S.C. (2014) 'Effect of material microstructure and tool geometry on surface generation in single point diamond turning', *Precision Engineering*, Vol. 38, No. 3, pp.481–491.

TOPSIL (2013) *High Transmission Silicon (HiTranTM) for Infrared*, TOPSIL, Ed.

Yan, J., Asami, T., Harada, H. and Kuriyagawa, T. (2009) 'Fundamental investigation of subsurface damage in single crystalline silicon caused by diamond machining', *Precision Engineering*, Vol. 33, No. 4, October, pp.378–386.

Yan, J., Asami, T., Harada, H. and Kuriyagawa, T. (2012) 'Crystallographic effect on subsurface damage formation in silicon microcutting', *CIRP Annals-Manufacturing Technology*, Vol. 61, No. 1, pp.131–134.

Yan, J., Syoji, K. and Kuriyagawa, T. (1999) 'Effects of cutting edge geometry on brittle-ductile transition in silicon machining', *Proceedings of the 9th International Conference on Precision Engineering (ICPE)*, Osaka, Japan, pp.92–97.

Yan, J., Syoji, K., Kuriyagawa, T. and Suzuki, H. (2002) 'Ductile regime turning at large tool feed', *Journal of Materials Processing Technology*, Vol. 121, No. 2, pp.363–372.

Yan, J., Yoshino, M., Kuriagawa, T., Shirakashi, T., Syoji, K. and Komanduri, R. (2001) 'On the ductile machining of silicon for micro electro-mechanical systems (MEMS) opto-electronic and optical applications', *Materials Science and Engineering a-Structural Materials Properties Microstructure and Processing*, Vol. 297, Nos. 1–2, January 15, pp.230–234.

Yan, J., Zhang, Z. and Kuriyagawa, T. (2001) 'Mechanism for material removal in diamond turning of reaction-bonded silicon carbide', *International Journal of Machine Tools and Manufacture*, Vol. 49, No. 5, pp.366–374.

Yan, J., Zhao, H. and Kuriyagawa, T. (2009) 'Effects of tool edge radius on ductile machining of silicon: an investigation by FEM. *Semiconductor Science and Technology*, Vol. 24, No. 7, p.075018.

Yergök, Ç. (2010) *Rough Cutting of Germanium with Polycrystalline Diamond Tools*, Master of Science Thesis, Mechanical Engineering Department, Middle East Technical University, Ankara.

Yuan, J., Lyu, B., Hang, W. and Deng, Q. (2017) 'Review on the progress of ultra-precision machining technologies', *Frontiers of Mechanical Engineering*, pp.1–23.

Zhang, S.J., To, S., Wang, S.J. and Zhu, Z.W. (2015) 'A review of surface roughness generation in ultra-precision machining', *International Journal of Machine Tools and Manufacture*, Vol. 91, pp.76–95.

Zhang, X., Woon, Ks. and Rahman, M. (2014) '11.09 diamond turning', in Hashmi, S. (Ed.): *Comprehensive Materials Processing*, 1st ed., Elsevier, Amsterdam, pp.201–220.

Zhang, Z. and Zheng, H. (2009) 'Optimization for decolorization of azo dye acid green 20 by ultrasound and H2O2 using response surface methodology', *Journal of Hazardous Materials*, Vol. 172, Nos. 2–3, pp.1388–1393.

Zhong, Z. (2003) 'Ductile or partial ductile mode machining of brittle materials', *The International Journal of Advanced Manufacturing Technology*, Vol. 21, No. 8, pp.579–585.

Zhou, M., Ngoi, B.K.A., Zhong, Z.W. and Chin, C.S. (2001) 'Brittle-ductile transition in diamond cutting of silicon single crystals', *Materials and Manufacturing Processes*, Vol. 16, No. 4, pp.447–460.

Website

Jmp, S.D., From Sas. (10 May). *Lack of Fit*. Available: https://www.jmp.com/support/help/14/lack-of-fit.shtml

Transformations: An Introduction, 10 May. Available: http.//fmwww.bc.edu/repec/bocode/t/transint.html